CrossMark

Thermally Activated Slip in Rare Earth Containing Mg-Mn-Ce Alloy, ME10, Compared with Traditional Mg-Al-Zn Alloy, AZ31

VIKAAS BAJIKAR,[1] JISHNU J. BHATTACHARYYA,[1,2]
NATHAN PETERSON,[1] and SEAN R. AGNEW[1]

1.—University of Virginia, Charlottesville, VA 22904-4745, USA. 2.—e-mail: jjb4cp@virginia.edu

It is of interest to assess the thermally activated nature of the deformation mechanisms responsible for the anisotropic response of textured Mg alloys, especially in those alloys that do and do not contain rare earth elements. The repeated stress relaxation method in combination with elasto-viscoplastic self-consistent (EVPSC) polycrystal modeling is employed to determine the strain rate sensitivity and true activation volume of samples of textured, polycrystalline Mg alloys, ME10 and AZ31, loaded along different directions in both the hard-rolled (F) and annealed (O) tempers. The results of Haasen plot analyses suggest that a superposition of at least two key mechanisms is responsible for controlling the thermally activated motion of dislocation for both of the alloy types investigated. One has a lower activation volume (solute-dislocation interaction and/or cross-slip), while the other is the ever-present forest dislocation interaction.

INTRODUCTION

An accurate description of the strain rate and temperature dependence of the flow stress of a metallic alloy is of utmost importance to engineers interested in alloy design, thermomechanical processing, formability and application. In the paradigm of dislocation slip-based crystal plasticity, the flow stress is often considered to be composed of athermal and thermally activated components.[1,2] The former is essentially independent of strain rate and temperature (except a weak dependence due to the temperature dependence of the elastic constants) and results from long-range elastic interactions of dislocations with obstacles, where thermal energy is insufficient to overcome the activation barrier. The latter represents the stress required by the dislocations to overcome local energy barriers, where thermal energy can aid the process. Hence, this latter portion is a strong function of strain rate and temperature and is essentially responsible for all the rate and temperature dependence of flow stress.

Thermally activated slip has been studied in great detail for cubic materials (both single and polycrystals) where often only one slip mode is of interest. Contrary to cubic materials, hexagonal close-packed (hcp) materials such as Mg have multiple slip modes, which are active for a given strain path. Under such conditions, the polycrystal-to-slip system level transition is not so straightforward, as the relative activities of the slip modes affect the macroscopic response. There have been far fewer studies of thermally activated slip in Mg and its alloys. Some noteworthy exceptions are the single-crystal studies of basal slip by Conrad et al.[3,4] and of prismatic slip by Couret and Caillard.[5,6] The behavior of single-crystal solid solution alloys was carefully examined by Amadieh et al.[7] and Akhtar and Teghtsoonian.[8,9] The latest of these was performed in 1985.

Regarding polycrystals, a study of pure Mg was carried out by Sastry et al.[10] A number of alloys were examined by Lukac, Trojonova and their collaborators.[11,12] In these studies of polycrystals, hcp Mg and its alloys were treated as others have treated fcc materials in which there is a single active slip mode, and it is often assumed that a single Schmid or Taylor factor is sufficient to relate polycrystal measurements to the dislocation-scale thermally activated events of interest. In this article, the thermally activated response is measured using a repeated stress relaxation method, which is less susceptible to problems associated

with machine compliance and changes in the mobile dislocation density compared with traditional stress relaxation methods.[2] In addition, an elasto-viscoplastic self-consistent (EVPSC) polycrystal model is used to calculate a factor based upon the relative activity of the various slip modes.

BACKGROUND

The plastic shear rate, mobile dislocation density and dislocation velocity are related according to the Orowan equation:

$$\dot{\gamma} = \alpha \rho_m b v \qquad (1)$$

where α is a geometric factor, b is the Burgers vector, ρ_m is the mobile dislocation density, and v is the velocity of dislocations. The latter is often modeled as an Arrhenius equation:

$$v = v_g \Lambda \exp\left(\frac{-\Delta G(\tau^*)}{kT}\right) \qquad (2)$$

where ΔG is the stress-dependent activation free energy, v_g is the attempt frequency ($\sim 10^{11}$ Hz), and Λ is the mean free path. The flow stress dependence on the strain rate ($1/m$) at any temperature T can be obtained from Eqs. 1 and 2 as:

$$\frac{1}{m} = \frac{\partial \ln \dot{\gamma}}{\partial \ln \tau}\bigg]_{T,s} = \alpha b v_g \frac{\partial \ln(\Lambda \rho_m)}{\partial \ln \tau}\bigg]_{T,s} - \frac{\tau}{kT}\frac{\partial \Delta G}{\partial \tau}\bigg]_{T,s} \qquad (3)$$

Frequently, $-\frac{\partial \Delta G}{\partial \tau}$ is denoted as the activation volume, $V = Ab$, where A is known as the activation area, i.e., the critical area swept during a thermally activated event.

The repeated stress relaxation method was applied to determine the thermally activated parameters m and V.[2] As the material is held at a constant total strain, the elastic strain relaxes, which is compensated by an increase in plastic strain. In repeated relaxation tests, this procedure is performed multiple times on a single specimen where the machine compliance effects are eliminated and an elastic reloading ensures that the dislocation density at the end of one relaxation is the same before the start of the next relaxation.[13]

A function commonly used to describe the decrease in stress over time for a single relaxation is the logarithmic model:

$$\Delta \tau = \left(\frac{-kT}{V_a}\right) \ln\left(1 + \frac{t}{c}\right) \qquad (4)$$

where V_a is the apparent activation volume and c is a time constant. Taking the time derivative of this equation yields the stress and strain rate during relaxation. It is noted that numerous functions have been employed for this purpose, including power law,[14] hyperbolic and hyperbolic sine.[15] Examining the distinctions between these approaches is beyond the scope of the present article; however, it is noted that Eq. 4 only has two fitting parameters and yields goodness of fit values that are as good as or better than the other options.

To discern the true activation volume, repeated relaxation data can be used to calculate a correction factor Ω, such that $V = V_a/\Omega$. Ω is given by:[2,13]

$$\Omega^{-1} = 1 - \left(\frac{kT}{V_a \sum_1^{n-1} \Delta \tau_j}\right) \ln\left[\frac{\exp\left(\frac{-V_a \Delta \tau_n}{kT}\right) - 1}{\exp\left(\frac{-V_a \Delta \tau_1}{kT}\right) - 1}\right] \qquad (5)$$

where n is the nth relaxation in the series. This equation provides four values of Ω for a series of five relaxations, and thus for every repeated relaxation test four values of the activation volume are obtained. The assumptions made in order to derive this are as follows: the dislocation motion is thermally activated (Eq. 2); the microstructure of the specimen is constant between successive relaxations as the material is reloaded elastically; the relaxation occurs only in the specimen and not in the machine.[13] In this study, the repeated stress relaxation method was applied over a range of pre-strain levels as part of an effort to examine the validity of the Cottrell-Stokes law for Mg and its alloys.[16]

METHODS

Material and Initial Microstructure

Two commercial Mg alloys, ME10 (Mg—1 wt.% Mn—0.4 wt.% Ce) and AZ31 (Mg—3 wt.% Al—1 wt.% Zn), were used for this study. The composition of the ME10 alloy was confirmed using x-ray fluorescence spectroscopy. The test specimens were punched from rolled sheets into ASTM sub-size standard specimens, which have a 25-mm gauge section. Both alloys were received as hard-rolled (F-temper) sheets of 1 mm thickness. The ME10 samples were annealed at 400°C for 2 h, and the AZ31 samples were annealed at 345°C for 1 h (to yield the O temper).

Samples were polished along the RD/TD plane for optical microscopy with standard metallurgical procedures down to 0.5 μm colloidal silica and etched with acetal-picric etchant.

For texture analysis, 3×3 cm^2 samples were sheared from material sheets and polished with metallurgical papers down to 1200 grit. Three pole figures, $(10\bar{1}0), (0002), (10\bar{1}1)$, were collected in Schulz reflection geometry on an X'Pert PRO MPD using CuKα radiation at 45 kV/40 mA up to 80° in χ. After background and defocusing corrections, the orientation distribution was calculated from the experimental pole figures using the MTEX library for MATLAB© with standard settings.

Mechanical Testing

Tensile tests along the rolling direction (RD), transverse direction (TD) and at 45° in-plane from RD (45) of the sheet material were conducted on an MTS Sintech 10/GL universal testing machine at room temperature in air. Load data were taken from a 50-kN load cell, and strain was measured using an Epsilon 3542 extensometer. All tests were

conducted with constant crosshead velocity corresponding to a nominal strain rate of 10^{-4}–10^{-1} s^{-1}. Specimens were pre-loaded to $\sim$ 7 MPa before the extensometer was attached. The plastic strain anisotropy (r values) was measured at 10% strain following the procedure described in earlier works.[17–19] Strain rate jump tests were conducted by changing the crosshead velocity corresponding to changes in strain rate ($\dot{\varepsilon} = 10^{-3}$ s^{-1} $\rightarrow$ 10^{-1} s^{-1} $\rightarrow$ 10^{-3} s^{-1} $\rightarrow$ 10^{-5} s^{-1} $\rightarrow$ 10^{-3} s^{-1}) at predefined strain levels. The strain between the jumps was large enough to dissipate transient effects and attain steady state.

For repeated stress relaxation tests, the given specimen was deformed at a constant nominal strain rate until a certain stress value was reached after which the crosshead was stopped and the specimen was allowed to relax for 30 s before it was reloaded at the same strain rate up to the same stress level. This procedure was carried out at multiple strain (stress) levels, ensuring that the strain levels did not exceed the uniform elongation limit. The analysis of the relaxation data was carried out as described in the background section. Note that it is known that twinning contributes very little strain during tensile deformation of Mg alloys with textures like the samples examined in this study, e.g., Refs. 20 and 21; therefore, the analysis that follows is focused on dislocation slip accommodated plasticity.

Crystal Plasticity Modeling

An in-house version of the elasto-viscoplastic self-consistent (EVPSC) code, similar to that of Wang et al.[22], was used to model the flow curves, r values and texture evolution of both ME10 and AZ31 alloys. In all cases, the initial texture was discretized into 2000 grains, and appropriate boundary conditions for uniaxial tension tests were imposed. The Taylor factor M is used to connect the shear quantities at the grain level to those measured at the polycrystal/macroscopic level. The expression for this Taylor factor, the volume-weighted ratio of the total accumulated shear rate $\bar{\bar{\Gamma}}$ to the norm of the total plastic strain rate in a grain $\dot{\varepsilon}$ modified for uniaxial case, is given by:[23]

$$M = \frac{\bar{\bar{\Gamma}}}{\|\dot{\varepsilon}\|} = \frac{\sum_g \sum_s \dot{\gamma}^{s,g} w^g}{\sqrt{1.5}\|\dot{\varepsilon}_p^g\|} \qquad (6)$$

where $\dot{\gamma}^{s,g}$ is the shear rate of a given slip mode in a grain and w^g is the volume fraction of the corresponding grain. The Taylor factors obtained from the model varied slightly as a function of alloy, strain level and straining direction, albeit only from 2.1 to 2.25. In what follows, a value of 2.1 was employed in all of the activation volume calculations. Note, implicit in the definition is the assumption that the critical resolved shear stresses are the same for all the modes in all of the grains. This is
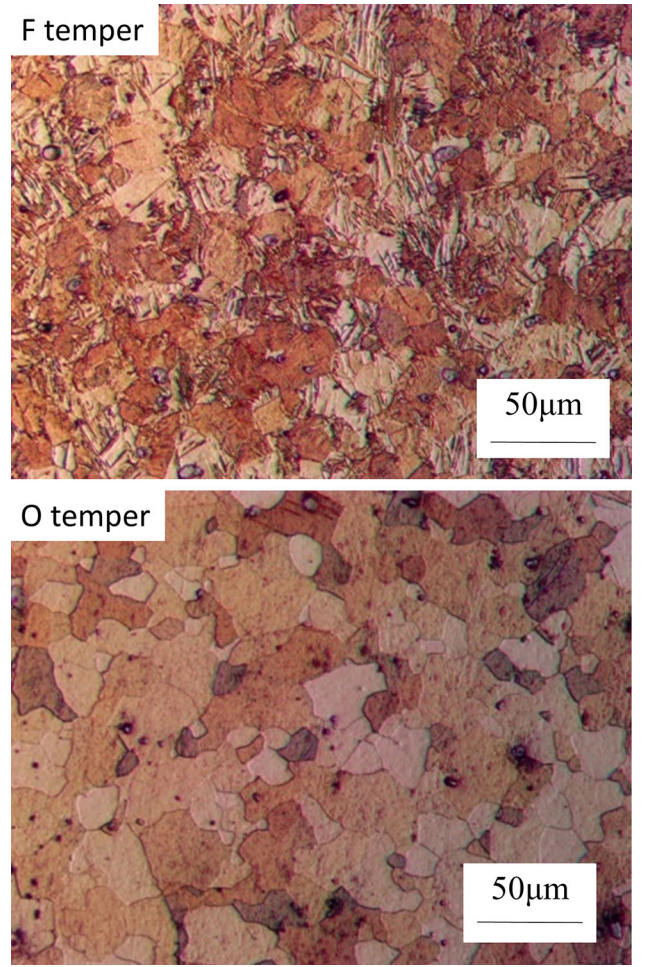

Fig. 1. Microstructure of alloy ME10 in the as-rolled (F) and annealed O temper (annealed at 400°C, 2 h).

more appropriate for face-centered cubic crystals of interest in Taylor's original work than it is in the present case where both basal (soft) and non-basal (hard) modes are known to be active. The importance of this simplifying assumption will be the subject of future work.

RESULTS

Initial Microstructure

The as-rolled ME10 alloy exhibits twins, whereas the annealed material is essentially free of twins, and the lineal intercept grain sizes were found to be 15 μm and 20 μm, respectively (Fig. 1). The microstructure of the rolled and annealed AZ31 is not shown in the interest of space. They are typical of commercially produced material.[24]

The basal texture typical of as-rolled Mg alloys is shown for ME10 in Fig. 2, as well as the annealed material, which shows a weaker basal texture typical of binary Mg-rare earth alloys, indicating that ternary additions of Mn do not have the strong synergistic effect with rare earth elements that has been reported for Mg-Zn-rare earth alloys and
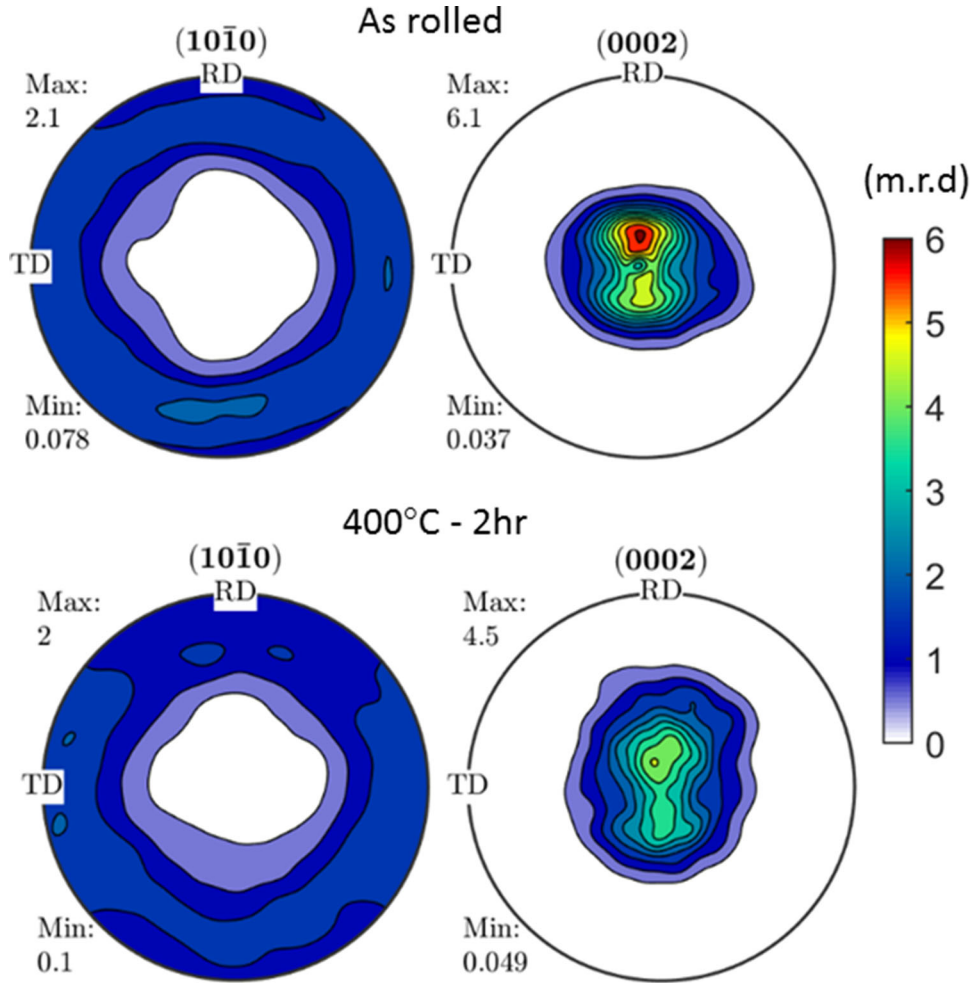
Fig. 2. Recalculated (10$\bar{1}$0) and (0002) pole figures of alloy ME10 in as-rolled (F) and O temper (annealed at 400°C, 2 h).

results in a strong splitting of the basal poles toward the TD.[25]

Mechanical Testing

Figure 3 shows the true stress–strain curves at a strain rate of 10^{-3} s^{-1} of the as-received and 2-h annealed ME10 alloy. Interestingly, the yield stress along the different directions for the as-received condition is the same; however, the strain-hardening response is anisotropic, with flow softening evident along RD. The annealed material has a lower strength and higher ductility, as expected, and shows a remarkably isotropic response for both yield stress and strain hardening. (Again, the stress strain response of the AZ31 material is typical and therefore not shown in the interest of space.) The r values in as-received as well as annealed ME10 were in the range of 0.91–1.35 (depending on RD, TD or 45 direction), which is quite different from that observed in AZ31 (r value of 3.5 along TD). Also shown in these figures are the results of EVPSC polycrystal modeling, which captures the differences between ME10 and AZ31, which are shown to

be the result of the initial texture and relative strengths of the basal and non-basal slip systems (Table I). Monotonic tensile tests carried out at different strain rates and strain rate jump tests were used to determine the strain rate sensitivity, m, defined in Eq. 3 (see Table II). All of the stress relaxation and strain rate jump test data reported henceforth were obtained from tests of TD-oriented samples. Tests performed along the other sample directions (RD and 45) revealed no significant difference in the activation volume or rate sensitivity and hence are not shown in the interest of space.

Figure 4 shows a typical true stress–strain curve for a repeated relaxation test, where relaxations were carried out at four different strain levels. With each reloading, the amount of relaxation decreases because of the exhaustion of the mobile dislocation density. Note that the reloading is not entirely elastic, as seen from the deviation from linearity. The impact of this deviation from standard practice will be examined in a future study. Figure 4 also shows an example of the logarithmic fit of the initial relaxation data to obtain the apparent activation volume, V_a. Typical goodness of fit values of
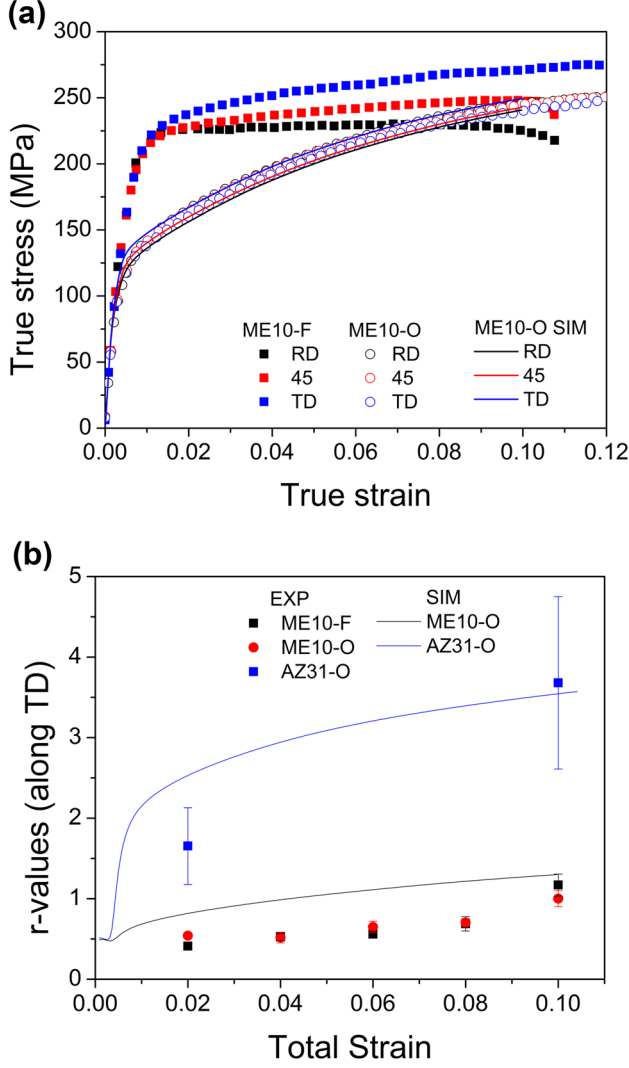
(a)

(b)

Fig. 3. (a) Experimental flow curves of ME10-F and O temper, with EVPSC simulation results for O temper (b) experimental and simulated r values along TD for ME10-O and AZ31-O.

Table I. Voce hardening parameters employed in the EVPSC model for ME10-O and AZ31-O

Def. mode	$\tau_{i,0}$ AZ31-O	$\tau_{i,0}$ ME10-O	$\tau_{i,1}$ AZ31-O & ME10-O	$\theta_{i,0}$ AZ31-O & ME10-O
Basal	30	20	30	300
Prismatic	90	75	40	300
$<c + a>$	120	120	50	500
TTW	40	40	0	55

Table II. Strain rate sensitivity data obtained from flow stresses at a fixed strain during multiple tensile tests, during rate jump tests and from the slope of the Haasen plot obtained from stress relaxation

Alloy	Multiple tests	Rate jump	Haasen plot
ME10 AR	0.0162	0.0183	0.017
ME10 O	n/a	0.017	0.021
AZ31 O	0.01*	0.0187	0.008

*AZ31O data obtained from Ref. 24.

Hence, as $\sigma \rightarrow 0$, $V \rightarrow \infty$, i.e., the Haasen plot passes through the origin. Moreover, if the Cottrell-Stokes relation holds, then the Haasen plot is a straight line with a constant slope, which is related to the strain rate sensitivity, m.

In the presence of another mechanism whose activation volume is lower (denoted here as V_s) compared with forest interactions, and its strengthening contribution, σ_s, follows a linear superposition (such may be the case for lattice resistance, solute-dislocation interactions or cross-slip), then it can be shown [26] that the overall activation volume is given by:

$$\frac{1}{V} = \frac{1}{V_s} + \frac{1}{V_s}\left(\frac{\sigma_d}{\sigma_s}\right) \quad (7)$$

In other words, both the slope and intercept of the Haasen plot would change because of the addition of this mechanism.

The strain rate sensitivity values, m_H, derived from the slope of the Haasen plot are shown in Table II. The slightly lower value of m_H obtained from the ME10 samples in F temper relative to those in O temper is consistent with the fact that the dislocation content in the former is higher than that in the annealed. The intercept values, on the other hand, are the same and equal to $(61b^3)^{-1}$. This suggests that in addition to the ever-present forest dislocation interactions, a single, more rate-sensitive mechanism operates in both conditions. This addition mechanism is most likely related to the solute-dislocation interaction (e.g., strengthening)

$R^2 = 0.99$ were obtained. The typical values of the correction factor Ω, defined in Eq. 5, was ~ 1.4, and the true activation volumes obtained are presented in Fig. 5. In the following section, these true activation volumes and their relationships to the rate-controlling mechanisms will be discussed.

DISCUSSION

To gain further insight into the rate-controlling mechanisms operative in these alloys, the so-called "Haasen plot" of inverse activation volume versus post-yield flow stress was calculated, as shown in Fig. 6, for ME10 in both F and O temper and for AZ31 in O temper. The basis of this plot is as follows. When only forest dislocation interactions are operative, the flow stress σ_d is inversely proportional to the average spacing of forest dislocations, l. It follows from the definition $V = -\frac{\partial \Delta G}{\partial \tau}$ that the activation volume V_d is directly proportional to l.
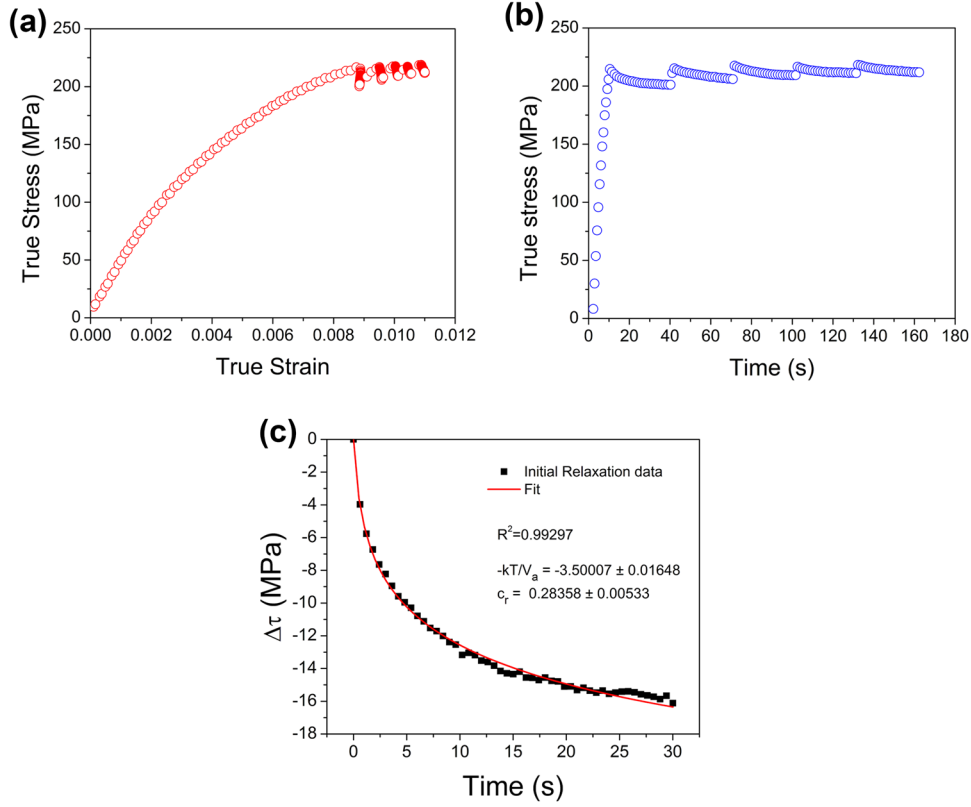
Fig. 4. (a) Stress/strain during a repeated relaxation experiment on ME10-F-TD, (b) stress as a function of time during a repeated relaxation experiment and (c) an example of the fit of the logarithmic model to the experimental data of change in stress ($\Delta\sigma$) versus time.
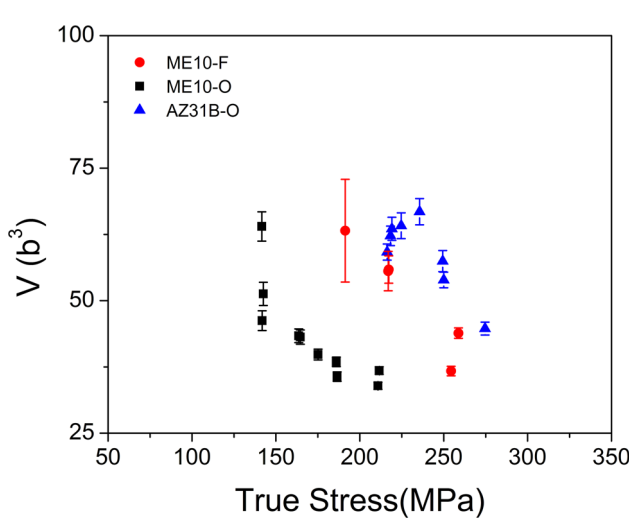

Fig. 5. True (physical) activation volume as a function of applied stress, as determined from repeated stress relaxation tests performed on TD samples of ME10-F, ME10-O and AZ31-O.
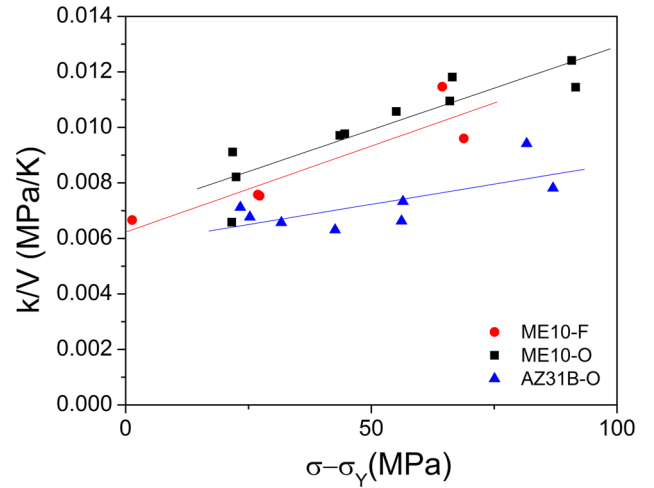

Fig. 6. Haasen plot for ME10 in the as-rolled (F) and annealed (O) tempers, i.e., inverse activation volume normalized by Boltzmann's constant, k, and plotted as a function of the flow stress minus the 0.002 offset yield stress.

and/or solute-influenced cross-slip, since the EVPSC modeling revealed that slip of $< a >$ dislocations on non-basal planes is a significant contributor to the strain accommodation.

Interestingly, the AZ31 alloy has a higher intercept value of $(76b^3)^{-1}$ and a lower rate sensitivity of 0.008. It is clear that the contribution of the second

mechanism is higher in case of AZ31 compared with ME10. For one thing, AZ31 has a much higher solute content (on a mole fraction basis) compared with ME10. Further work is being pursued to identify whether classical solute strengthening or solute-influenced cross-slip is the dominant mechanism.

At this point, it is worth mentioning the results of prior studies on pure Mg and its alloys to place the current results in context. Conrad et al. [4] obtained $V \sim 10^4 \; b^3$ for pure single crystal Mg, which is consistent with the fact that at very low stresses (which they investigated) the dislocation-forest interactions would lead to very high activation volumes. Similarly, Sastry et al.[10] also obtained values $\sim 10^2 \; b^3$ while investigating pure Mg polycrystals at low stress levels. As explained above, the intercept of the Haasen plot will be zero, i.e., the activation volume will become large, when forest dislocation interactions are the only thermally activated mechanism, as is observed for pure metals, e.g., Refs. [26] and [27]. As far as alloys are concerned, studies on the AJ, AX and AZ alloys have all yielded activation volumes in the same range as was observed presently for 50–100 b^3, if restricting one's attention to a similar stress level.[11,12,28] Future studies will seek to discriminate what the second mechanism is (in addition to forest interactions) and what its relationship to the evolving dislocation density is.

CONCLUSION

The repeated stress relaxation technique has been used to study thermally activated deformation of two commercial Mg alloys (ME10 and AZ31). Analysis of the obtained physical activation volume data using the Haasen plot has revealed adherence to the Cottrell-Stoke relation (constant strain rate sensitivity with straining). In addition to the forest dislocation interactions revealed to be rate controlling in previous studies of pure Mg single and polycrystals, the present analysis has highlighted the operation of another thermally activated mechanism, most likely associated with solute additions. Finally, because the different alloys exhibit distinct slopes in the Haasen plot, it is also suggested that the distinct solute elements and concentrations may play a role in controlling the sorts of dislocation structures that evolve with straining.

ACKNOWLEDGEMENTS

REFERENCES

1. U.F. Kocks, A.S. Argon, and M.F. Ashby, *Thermodynamics and Kinetics of Slip, Progress in Materials Science*, vol. 19, ed. B. Chalmers, J.W. Christ, and T.B. Massalsk (Oxford: Pergamon Press, 1975), pp. 1–288.
2. D. Caillard and J.L. Martin, *Thermally Activated Mechanisms in Crystal Plasticity (Pergamon Materials Series*, Vol. 8 (Amsterdam: Elsevier, 2003).
3. H. Conrad and W.D. Robertson, *Trans AIME* 209, 503 (1957).
4. H. Conrad, L. Hays, G. Schoeck, and H. Wiedersich, *Acta Metall.* 9, 367 (1961).
5. A. Couret and D. Caillard, *Acta Metall.* 33, 1447 (1985).
6. A. Couret and D. Caillard, *Acta Metall.* 33, 1455 (1985).
7. A. Ahmadieh, J. Mitchell, and J. Dorn, *Lithium Alloying and Dislocation Mechanisms for Prismatic Slip in Magnesium* (No. UCRL-11417 Rev. 2) (Berkeley: California University, Lawrence Radiation Lab, 1965), pp.1–34.
8. A. Akhtar and E. Teghtsoonian, *Acta Metall.* 17, 1351 (1969).
9. A. Akhtar and E. Teghtsoonian, *Acta Metall.* 17, 1339 (1969).
10. D.H. Sastry, Y.V.R.K. Prasad, and K.I. Vasu, *Curr. Sci.* 39, 97 (1970).
11. P. Lukac and Z. Trojanová, *Key Eng. Mater.* 465, 101 (2011).
12. Z. Trojanová, K. Máthis, P. Lukáč, G. Németh, and F. Chmelík, *Mater. Chem. Phys.* 130, 1146 (2011).
13. P. Spätig, J. Bonneville, and J.-L. Martin, *Mater. Sci. Eng. A* 167, 73 (1993).
14. J.C. Li, *Can. J. Phys.* 45, 493 (1967).
15. T. Kruml, O. Coddet, and J.L. Martin, *Acta Mater.* 56, 333 (2008).
16. A.H. Cottrell and R.J. Stokes, *Proc. R. Soc. Lond. A* 233, 17 (1955).
17. J.J. Bhattacharyya, F. Wang, P.D. Wu, W.R. Whittington, H. El Kadiri, and S.R. Agnew, *Int. J. Plast* 81, 123 (2016).
18. J.J. Bhattacharyya, S.R. Agnew, M.M. Lee, W.R. Whittington, and H. El Kadiri, *Int. J. Plast* 93, 46 (2017).
19. A. Jain and S.R. Agnew, *Mater. Sci. Eng. A* 462, 29 (2007).
20. H. Wang, B. Raeisinia, P.D. Wu, S.R. Agnew, and C.N. Tomé, *Int. J. Solids Struct.* 47, 2905 (2010).
21. A. Jain, O. Duygulu, D.W. Brown, C.N. Tomé, and S.R. Agnew, *Mater. Sci. Eng. A* 486, 545 (2008).
22. H. Wang, P.D. Wu, C.N. Tomé, and Y. Huang, *J. Mech. Phys. Solids* 58, 594 (2010).
23. U.F. Kocks, C.N. Tomé, and H.-R. Wenk, *Texture and Anisotropy: Preferred Orientations in Polycrystals and Their Effect on Materials Properties* (Cambridge: Cambridge University Press, 2000).
24. S.R. Agnew and Ö. Duygulu, *Int. J. Plast* 21, 1161 (2005).
25. J. Bohlen, M.R. Nürnberg, J.W. Senn, D. Letzig, and S.R. Agnew, *Acta Mater.* 55, 2101 (2007).
26. W.A. Curtin, *Scr. Mater.* 63, 917 (2010).
27. R.A. Mulford, *Acta Metall.* 27, 1115 (1979).
28. Z. Trojanová, P. Palček, P. Lukáč, and Z. Drozd, *Magnes. Alloy. Solid Liq. States* (2014), pp. 3–47.